

Power dissipation mechanisms in radio-frequency driven silane discharges: The influence of discharge geometry

D. Mataras, S. Cavadias, and D. Rapakoulias

Department of Chemical Engineering, University of Patras, P. O. Box 1407, GR-26500, Patras, Greece

(Received 2 June 1992; accepted 9 January 1993)

The influence of chamber geometry on the electron impact dissociation and dissociative excitation processes, in a capacitively coupled radio-frequency (rf) silane discharge, is presented. This is achieved by examining the influence of geometry, in conjunction with other macroscopic parameters, on the concentrations of ground state SiH and electronically excited SiH* radicals, recorded simultaneously by spatially resolved laser induced fluorescence and optical emission spectroscopy. The geometry of the discharge is modified, by changing either the interelectrode distance or the electrode diameters, whereas the electric symmetry of the discharge is monitored by the change of the self-bias direct-current potential of the rf electrode. Our observations indicate that the specific path and power consumption of the generation processes of the two radicals are spatially differentiated and sensitive to geometry variations. Thus, emission and fluorescence spatial intensity profiles are differently influenced. In the case of the modification of interelectrode distance, a redistribution of the energy consumed by each of the radical generating processes has been observed.

I. INTRODUCTION

Plasma enhanced chemical vapor deposition (PECVD) of α -Si:H and related alloys has been the subject of many studies in the last few years. The large and continuously growing number of applications of this family of materials in the fabrication of various electronic devices, has stimulated research activities concerning the fundamental aspects of this process, as well as reactor design, characterization of the films, efficiency, and stability of α -Si based devices.

However, the present situation is largely characterized by a semiempirical approach in understanding and controlling the process. This is because a direct relation between the properties of the deposited film and the entire set of externally controllable parameters is not yet achievable.

In this context, considerable attention has been paid to the identification of possible growth precursors and their role in elementary gas-phase and surface processes, in an effort to correlate macroscopic plasma parameters to the film properties by means of a properly formulated mechanism.

Plasma diagnostics have already played an important role in providing insight and data for a realistic simulation of these elementary processes. Thus, besides the identification of active species,¹⁻³ we have now some information about their number density^{4,5} and behavior⁶ during the deposition of α -Si:H.

However, there are still many open questions, which originate from the fact that most of the microscopic properties of these discharges are spatially and temporally dependent, while most often only the energy dependence, of the time and space averaged properties, is taken into account.

These microscopic plasma properties are related to the basic discharge-sustaining mechanisms associated with the specific power consumption of ionization, dissociation, ex-

citation, and other gas phase collision processes. Therefore they are influenced by all the externally controllable parameters. Namely, they are most sensitive to the magnitude, frequency and coupling characteristics of rf power, and also pressure, flow rate, gas composition, and discharge geometry.

This last parameter is very important because it influences directly, as well as indirectly through its interdependence with other process parameters, the values of electric field and power density, and the discharge sustaining mechanism.⁷ However, the discharge geometry, and its correlation with gas phase and surface processes in gas discharges, has not been studied systematically. Only few works have partially addressed this subject,⁸⁻¹¹ despite its obvious importance.¹²

Thus, if the basic geometric characteristics of the chamber (electrode shapes and diameters, interelectrode spacing) are modified, the values of the sheath and plasma potentials are changed along with the time-averaged shape and magnitude of the bulk plasma and the electrode sheaths. Consequently, the specific power consumption of each elementary process, at each one of these discharge areas, will be significantly influenced.

Optical diagnostics have proven their sensitivity to these variations, and therefore, provide a powerful tool for recording the effects of geometry on the production and space distribution of reactive intermediates.¹³⁻¹⁶

Based on this idea, we have used spatially resolved laser induced fluorescence (LIF) and optical emission spectroscopy (OES) in order to study the influence of discharge geometry on the power dissipation mechanisms, by monitoring the specific generation rates of SiH and SiH* radicals. Besides the fact that these measurements are the only direct, spatially sensitive, information available about silane discharges, as it will be shown SiH and SiH* can be considered as model species for the comparative estimation of the outcome of electron collisional dissociation and dis-

sociative excitation of silane and also of its energy and space dependence.

It was revealed in this study that discharge geometry has considerable effects on these elementary processes.

II. EXPERIMENT

The experimental arrangement and the diagnostic techniques used in the present work have been described in detail elsewhere.⁶ In this experiment, we use 2 sets of round stainless-steel electrodes, 1 pair of 10 and 1 of 6 cm in diameter, in a 16 cm wide cylindrical stainless-steel deposition chamber. Both, the chamber and the deposition electrode are grounded.

The rf electrode is fixed, while the grounded one is mounted on a linear motion vacuum feedthrough that permits continuous adjustment of the interelectrode distance (between 0 and 70 mm) without interruption of the experiment. The powered electrode, equipped with a stainless-steel grounded shield, is connected to the rf generator (13.56 MHz) through an *L*-type matching network via a blocking capacitor. Forward and reflected power is measured with a low-power SWR bridge (Hansen FS-5S). Since the probable power losses in the impedance matching network are unknown, rf voltage and direct-current (dc) floating potential are continuously monitored on an oscilloscope via a high impedance probe connected to the powered electrode.

The gas is fed by the center of the rf electrode through a porous disk. Upstream flow control, using mass flow controllers, and downstream pressure control, by means of a throttling valve, ensures independent variation of pressure and flow in our range of working conditions. LIF and OES axial profiles are recorded by moving the deposition chamber, as described in Ref. 6. It is necessary to note that this method is far more accurate and simple than the often used technique of moving the excitation and collection optics, since there is no need for repeating the very laborious alignment procedure. The signal acquisition method has been simplified very much by using a digital storage oscilloscope equipped with an averaging module (Lecroy 9400). The photomultiplier tube (PMT) signal obtained from a specific discharge region is converted to a digital wave form of 1000 ns amplitude. The average of 2000 such wave forms is integrated in time after the subtraction of the time-equivalent emission and scattered laser light wave forms. The entire procedure is automated by using a pc-based control program. The accuracy of the method has proven to be much more satisfactory than the usual boxcar averaging technique which is based on analog signal processing.

III. RESULTS

In the present work spatially resolved LIF and OES have been employed for the simultaneous detection of both fundamental and electronically excited states of silylidine (SiH and SiH*) radicals. These methods were used for recording of entire one-dimensional (1D) (axial) intensity

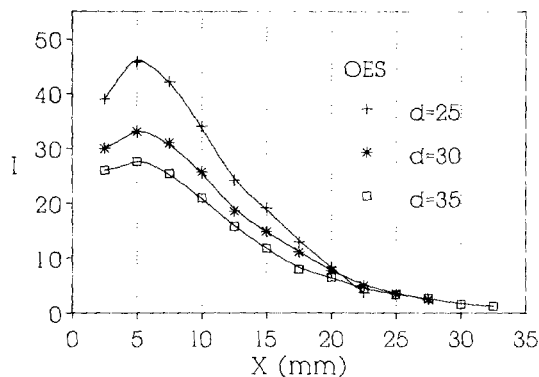


FIG. 1. Emission intensity (*I* in arbitrary units) as a function of the distance (*X*) from the powered electrode for three interelectrode distances (*d*). ($P = 50$ mTorr, $W = 12$ W, $f = 10$ sccm pure silane.)

profiles, between the two electrodes, or for recording intensity variations at specific areas of particular interest in the interelectrode gap.

In the following, we will present the effects of interelectrode distance and electrode area on the space dependent generation of these radicals.

The first attempt was to modify the chamber geometry by moving one of the electrodes, namely the grounded one (momentary anode), in order to see how this affects the spatial intensity distribution of SiH and SiH* radicals.

Thus, in Figs. 1 and 2, are presented OES and LIF profiles, for three specific interelectrode distances (*d*), while maintaining all the other parameters constant.

A first observation is that the intensity maximum on both sets of curves does not change location (remains constant at $x = 10$ mm for LIF and $x = 5$ mm for OES). However, the total intensity of each curve shifts up as the two electrodes come closer.

The observed overall intensity shift is easily explained, since the power/cm³ ratio increases as the total power supplied to the discharge by the rf generator remains constant ($W_S = W_{\text{forward}} - W_{\text{reflected}}$). Consequently, fewer silane molecules are subject to a higher number of inelastic col-

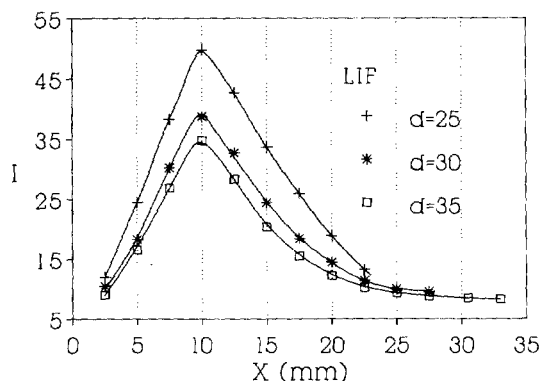


FIG. 2. LIF intensity (*I* in arbitrary units) as a function of the distance (*X*) from the powered electrode for three interelectrode distances (*d*). Same conditions as in Fig. 1.

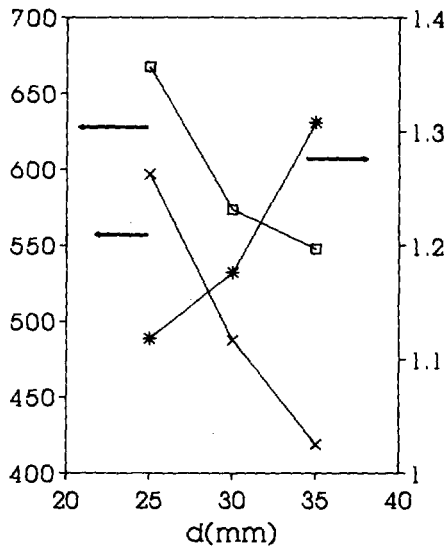


FIG. 3. Overall intensity I_{LIF} (\square) and I_{OES} (\times), and their ratio I_{LIF}/I_{OES} ($*$), obtained by integration of the LIF and OES curves from Figs. 1 and 2.

lisions with fast electrons and this results in higher densities for all kinds of radicals.

If the power density were homogeneous in space (in a discharge consisting only of a positive column), one would expect that the total increase, which can be calculated as

$$I_{(LIF,OES)} = \int_0^d I(x) dx,$$

where $I(x)$ the normalized LIF or OES intensity profile should scale approximately with d^{-1} . However, this is not observed experimentally. Indeed, as it can be seen in Fig. 3, the total LIF and OES intensities increase both with decreasing d , however, the specific rate of increase of each intensity is different. Namely, the ratio I_{LIF}/I_{OES} decreases as the interelectrode distance becomes shorter. This behavior suggests a redistribution of the specific power consumption between dissociation and dissociative excitation processes in favor of the latter.

These observations must be related to the variation of the contribution of the sheath and bulk plasma specific volumes to the overall discharge volume, but in addition one has to consider also the alteration of the discharge symmetry due to the contribution of other grounded surfaces. The major contribution coming from the grounded chamber walls can be estimated by measuring V_{dc} (the self-bias dc potential of the powered electrode with respect to the ground), which rises as a consequence of the current drawn by the blocking capacitor.^{17,18} If the ratio of the powered area (A_{rf}) to the grounded one (A_g) is defined as $R = A_{rf}/A_g$, then

$$V_{dc} = (1 - R^{-n}) \bar{V}_p,$$

where $\bar{V}_p = (1/2)(V_{dc} + V_{rf})$, the average plasma potential and n is a little higher than or equal to 1.

The value of V_{dc} can be used as a criterion of the discharge symmetry and as a reference for the evaluation of

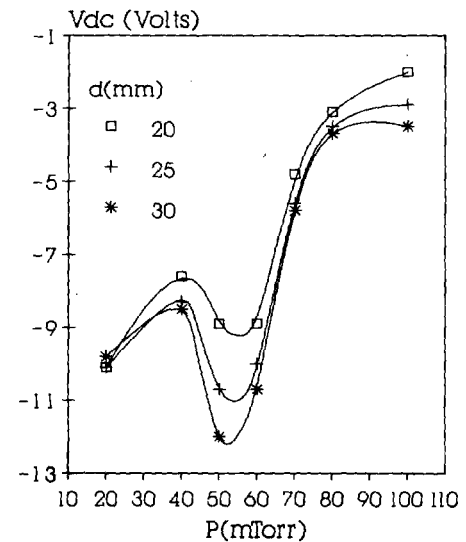


FIG. 4. Self-bias dc potential (V_{dc} in volts) of the rf electrode as a function of pressure, at three interelectrode distances (d) ($V_{rf} = 73$ V.)

spectroscopic measurements; when the discharge is approaching electrical symmetry, V_{dc} tends to 0 (since $R = 1$), whereas in the case of asymmetric discharges it has a negative value. This value rises as the discharge becomes more asymmetric. For example in Fig. 4 are presented characteristic V_{dc} curves as a function of pressure, for three different interelectrode distances. There is a clear tendency toward electric symmetry for pressures higher than 90 mTorr. However, one can also observe a minimum in the range of 20–50 mTorr.

Additionally, since the positions of LIF and OES maxima do not vary with interelectrode distance (Figs. 1 and 2), the intensity shift at the maximum can be used for recording the influence of d in a more extended range, simultaneously with V_{dc} .

Thus, Fig. 5 presents the variation of LIF and OES intensities recorded at I_{max} 10 mm from the rf electrode, together with V_{dc} .

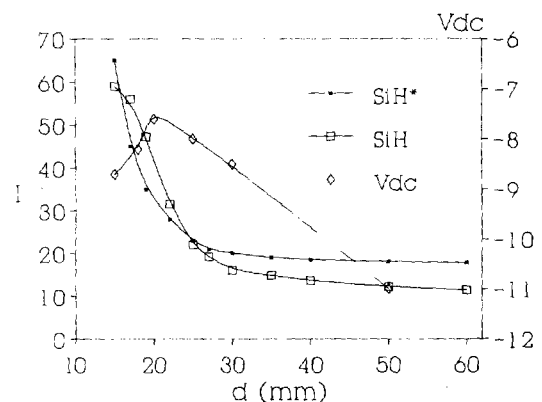


FIG. 5. LIF and OES intensity (I in arbitrary units) together with V_{dc} (in volts) as a function of interelectrode distance (d). Both intensities are recorded at $X = 10$ mm from the rf electrode. ($P = 40$ mTorr, $W = 10$ W, $f = 11$ sccm pure silane, $V_{rf} = 73$ V.)

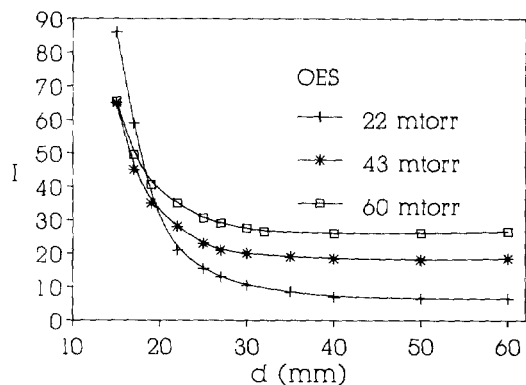


FIG. 6. Emission intensity (I in arbitrary units) as a function of interelectrode distance, recorded at $X = 10$ mm, for three different pressures. ($W = 12$ W, $f = 11$ sccm pure silane.)

Two main regions can be distinguished in this family of curves:

(i) for $d > 27$ mm where the effective grounded area includes much of the surrounding chamber walls, resulting in higher values of V_{dc} .

(ii) for $d < 27$ mm where the effective grounded area is approximately equal to the surface area of the grounded electrode, characterized by a sharp linear increase in both intensities and a decrease of V_{dc} .

The influence of the surrounding walls is much more important at low pressures, where the discharge spreads out, than in higher pressures when it is restricted near the electrodes and the electrons tend to be trapped in the bulk.

This can be observed in Figs. 6 and 7, where the same type of OES and LIF curves are plotted for three different working pressures.

In these figures, one can also observe the dependence of both intensities on pressure. Namely, emission intensity increases, while LIF intensity decreases with increasing pressure. In fact, there is a linear dependence in this range of pressures. Thus, in region I of these curves, intensity (I_{max} , at $X = 10$ mm from the rf electrode) is proportional

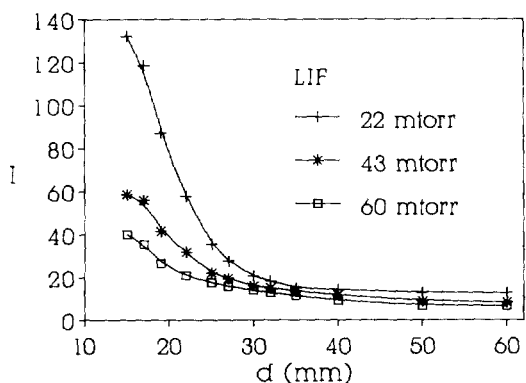


FIG. 7. LIF intensity (I in arbitrary units) as a function of interelectrode distance, recorded at $X = 10$ mm, for three different pressures. (Same conditions as in Fig. 6.)

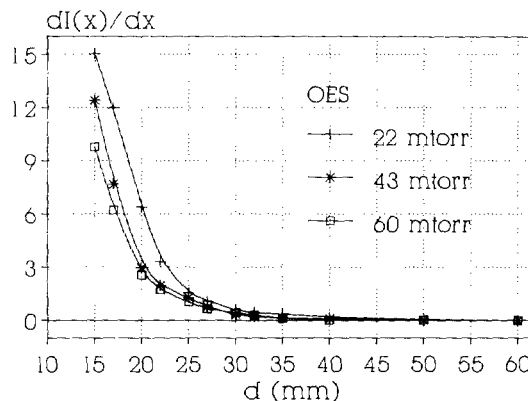


FIG. 8. Plot of $r_{em} = dI(x)/dx$ as a function of interelectrode distance (d).

to Pd^{-1} for emission and $P^{-1}d^{-1}$ for LIF, whereas in region II it is proportional to Pd^{-2} for emission and $P^{-1}d^{-2}$ for LIF, approximately.

Additionally there is a tendency for saturation of the LIF intensity curves as the interelectrode distance becomes very short ($d < 20$ mm).

To illustrate this last phenomenon, we have plotted the rate of increase of the concentration of each radical versus d in Figs. 8 and 9. This can be calculated as $r_{(em,LIF)} = [dI(x)]/dx$, the first derivative of intensity as a function of distance, giving r_{em} (rate of increase of emission intensity) and r_{LIF} (rate of increase of LIF intensity).

It is observed in these figures that r_{em} starts to increase at distances shorter than 50 mm (approximately equal to the distance of electrodes from the chamber walls [$(D - d)/2 \approx 50$ mm]), whereas the inflection point of these curves varies from ≈ 21 to ≈ 24 mm depending on pressure.

r_{LIF} also increases for $d < 50$ mm and presents an inflection point at ≈ 27 mm, the position of which does not depend on pressure. However, the r_{LIF} curve presents also a maximum for $d \approx 20$ mm when the rate of increase starts to drop again. This maximum appears at the same d where

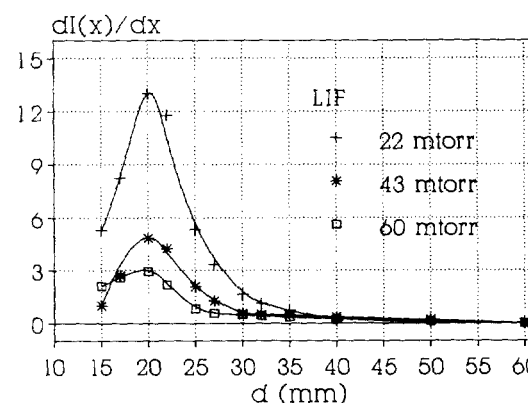


FIG. 9. Plot of $r_{LIF} = dI(x)/dx$ as a function of interelectrode distance (d).

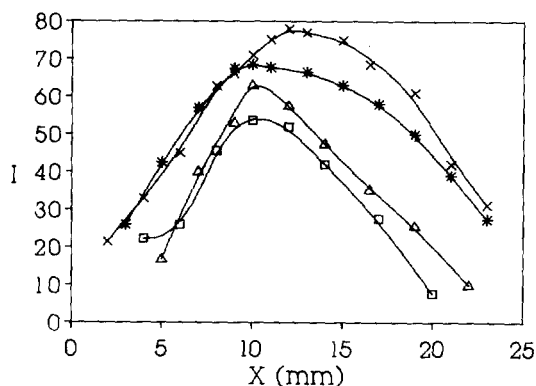


FIG. 10. LIF and OES intensity (I in arbitrary units) as a function of the distance (X) from the powered electrode, for two different area electrode sets. (a) (Δ) LIF and ($*$) OES for 6 cm cathode and 10 cm anode, (b) (\square) LIF and (\times) OES for 10 cm cathode and 6 cm anode ($P = 50$ mTorr.)

the value of V_{dc} is minimum (Fig. 5), and the discharge is more close to symmetry.

The results presented here clearly show that the two elementary processes (dissociation and dissociative excitation) are influenced differently by the variation of power density and discharge geometry.

To further illustrate this difference the diameters of the two electrodes were modified, thus modifying $R = A_{rf}/A_g$. This was accomplished by using 1 electrode of $D = 10$ cm and 1 of $D = 6$ cm diam.

(A) In the first case the big electrode is connected to the rf generator while the small one is grounded, (B) whereas in the second case the small electrode is powered and the big one is grounded ($R_A/R_B = 2.7$).

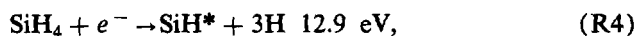
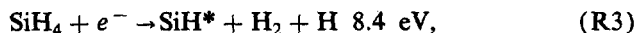
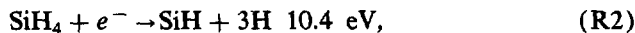
The results obtained (Fig. 10) show that the LIF maximum position is the same in both cases, unlike the emission maximum that is significantly influenced. More specifically, SiH^* concentration is higher in case (A) and dislocated toward the anode, while in case (B) is nearly flat in the center of the discharge.

Since our previous results do not indicate any such influence of pressure, power or any other parameter, this change is clearly attributed to the change in electrode diameters. Therefore, these observations indicate a close relation of SiH^* to the potential and magnitude of both cathode and anode sheaths. In the same time the concentration of SiH seems to be influenced only by the density of electrons in the bulk, which should be higher in case (B) (small rf electrode).

IV. DISCUSSION

In order to explain the different behavior of SiH and SiH^* species, it is necessary to outline the radical generation processes and all the various ways they can be influenced by the modification of interelectrode distance.

The two radicals are produced by one-electron inelastic collisions, as described in the following reactions (given with the theoretical radical formation thresholds):



$$k_5 = 3.3 \times 10^{-12} \text{ cm}^3 \text{ s}^{-1} \quad (\text{Ref. 1}).$$

After their generation electronically excited SiH^* radicals return spontaneously to the ground state by emitting a photon, whereas ground state SiH radicals react with silane toward Si_2H_5 [reaction (R5)]. The different dissipation path of the two radicals explains sufficiently the distinct response to the increase of pressure (Figs. 6 and 7). At higher pressures, the increased radical density enhances emission intensity, whereas the increased silane density affects only ground state radicals. Furthermore, (i) The rate of the reaction of ground state radicals with silane [reaction (R5)] is sufficiently high and overtakes diffusion at pressure > 25 mTorr.¹⁹ Our previous results⁶ indicate that the influence of diffusion is limited for pressures above 30 mTorr and not observable within the limits of experimental error for this pressure. (ii) Also, microscopically, the radicals will move with equal probability to all directions, despite the differences of the radical concentration in space. Thus, although the radical diffusion flux is determined by the gradient of the species this will not influence the measured LIF intensity at a single point of the discharge.

These arguments prove that the intensity at a specific location, and at sufficiently high pressure, will reflect the relative rate of generation of these radicals, since the concentration of silane is almost homogeneous in space at low depletion conditions.

Our previous measurements in the range below 30 mTorr, where diffusion effects are larger and should influence the LIF profiles, confirm this statement because the spatial profiles have the same shape (identical position I_{max}) in the range of 15–100 mTorr in pure silane and up to 0.5 Torr in diluted silane. If the ground state SiH radicals were generated according to a different spatial profile (as for example the OES profile) one would expect that actual concentration profiles, measured by LIF, would be strongly influenced by the modification of pressure. Nevertheless, the hypothesis of diffusion from an initial generation profile, identical with the emission profile, has also been checked by numerical calculations but failed to reproduce the experimental results.

Although SiH radicals represent a somewhat low percentage of the silane fragmentation pattern, there are strong indications that SiH spatial profiles represent the stationary silane fragment generation profiles not only for SiH but also for other low energy radicals as silylene (SiH_2) and silyl (SiH_3). Thus, considering the fact that most of the electron collisional dissociation of silane occurs by high energy (8–12 eV) electrons, (considerably higher than the mean electron energy and above the radicals' thermodynamic formation threshold²⁰) spatial generation profiles for SiH_2 and SiH_3 should be very close to that of ground state SiH . Still since these radicals are produced in

larger proportions, and their spatial distribution is determined by the specific reaction and diffusion rates of each radical, their actual *concentration profiles* can be different. However, actual measurements of SiH₃ profiles using infrared laser absorption revealed a noticeable similarity to SiH profiles.²¹ Namely the position of the maximum concentration is ~8–10 mm from the rf electrode ($d = 30$), but the distribution is much more uniform in space, compared to SiH, due to the much greater lifetime of this radical.

Therefore, an accurate estimation of the relative spatial abundance of each radical and their availability to surface processes is now possible to the extent that direct measurements of the density and behavior of these species (kinetic and transport coefficients) are available.

On the contrary, the case of electronically excited state SiH* radicals is different. Their spatial profiles present several differences compared to those of ground state SiH. Although they are also generated by one-electron collisions with silane, there is a considerable energetic difference ($\Delta E = 2.5$ eV, equations R1–R4) in their formation threshold, compared to their ground state counterparts. Accordingly, the experimentally determined appearance threshold of dissociative excitation (> 10.5 eV) is much closer energetically to dissociative ionization (> 11.9 eV) than to dissociation toward neutral radicals (> 8 eV).²² This difference, in conjunction with the spatial variation of the electron energy distribution function (eedf), which is caused by the anisotropy of the electron swarm, induces a dissimilar space distribution and behavior for SiH*, compared to SiH.⁶

Consequently, the different types of response of these two radicals, to energy, space, and density variations can lead to important conclusions, concerning the variation of the eedf and the power dissipation mechanisms in low pressure silane discharges.⁷

The variation of interelectrode distance while maintaining constant total power is affecting the generation process of these radicals in several ways. Namely, (a) when the two electrodes approach, the amount of power/cm³ increases thereby increasing the electron density. This causes a net increase in the concentration of the two species. It must be noted here, that the power density is usually calculated for the volume defined by the diameter of the electrodes neglecting sidewall effects. However, the experimental results shown earlier indicate clearly that the surrounding chamber walls can have a measurable influence, increasing at lower pressures, if they are located at distances comparable to the interelectrode distance.

(b) At the same time, the electron temperature increases,²³ at least for three reasons: First, because the contribution of hot γ electrons becomes larger, since the time-averaged volume of the sheaths is independent of d ; second, because bulk electrons are thermalized by the moving plasma-sheath boundary (wave-riding electrons);^{24,25} and third, because at short distances a hot electron flux is generated by interaction with the approaching anode sheath.²⁶

All these processes essentially modify the eedf, thus fa-

voring high energy processes against low energy ones.²⁷ Consequently, r_{em} is higher and linearly increasing, compared to r_{LIF} (Figs. 8 and 9). This is also supported by the fact that despite the observed decrease of emission intensity when pressure drops (Fig. 6), r_{em} is faster at lower pressures (Fig. 8), where the sheath potentials are higher resulting in faster γ electrons.

This is the cause of the redistribution of energy consumption between dissociation and dissociative excitation processes, as it is observed by the decrease of the I_{LIF}/I_{OES} ratio (Fig. 3).

(c) The net flux of electrons striking the surface of the two electrodes becomes larger at small d , leading to a decrease of the electron density.^{23,26} This is confirmed by the increase of V_{dc} (Fig. 5) and the decrease of r_{LIF} (Fig. 9) for distances below 20 mm. This phenomenon is more pronounced at lower pressures when there is a larger mean free path for electrons.

All the prior observations and arguments show a direct relation of the SiH* generation to the potential and the magnitude of the sheaths, whereas the generation of SiH is mainly influenced by the power density in the bulk.

The validity of this conclusion is enhanced by the experimental results concerning the modification of electrode area. In this case, the emission profile is always displaced towards the smaller electrode which presents the higher sheath potential, while the LIF profile is only affected by the power density which is higher in the small rf electrode case.

Also, this explanation is in good agreement with the phenomena observed in previous work of this group and justifies the explanations given there. Namely, ground state SiH profiles obtained by spatially resolved LIF measurements present a maximum located inside the bulk plasma (10 mm from the rf electrode), the position of which is insensitive to pressure, flow, composition of the feed gas, or interelectrode distance, while the spatial profiles of SiH* present a maximum that moves toward the rf electrode as pressure increases. The same effect can also be observed here by the crossing of the 22 mTorr OES curve with the other two pressure curves (Fig. 6). This is observed because these are single point measurements at the position of LIF intensity maximum (I_{max}). This is in accordance with the experimentally determined time-averaged sheath thicknesses, which decrease as pressure increases,²⁸ and the minimum V_{dc} observed in the range 20–50 mTorr (Fig. 4). If pressure increases above 100 mTorr a second intensity maximum appears near the anode. The same phenomenon has also been observed by Roth in nonreactive gases like N₂, H₂, Ar, and Ne. The displacement of the maxima and the shape of these profiles was found to depend on the nature of the gas.²⁹ He also observed that N₂ discharges present two intensity maxima (one near each electrode), while in the same conditions Ar and Ne present only one. Especially, H₂ has a similar behavior with silane; at low pressures it presents one maximum while a second one near anode appears at higher pressures. These observations have been experimentally reproduced by this group, and confirmed by other results that can be found in literature.^{30–32}

These changes in the emission profiles of gas discharges correspond to specific changes in the discharge sustaining mechanism. Namely, the first transition marked by the smooth displacement of the emission profile towards the rf sheath and the small minimum of V_{dc} (Fig. 4) corresponds to the electrode sheath confinement, while the appearance of the second intensity maximum and the sharp decrease in V_{dc} correspond to the transition from the α to the γ regime³³ which is characterized by an additional contribution of γ secondary electrons to the maintenance of the discharge.³⁴ The first transition occurs at a characteristic pressure for each gas, which in the case of pure silane lies between 20 and 50 mTorr, or the same silane partial pressure in the case of diluted silane.

Recently, Gallagher²⁰ and Kuznetsov³⁵ have used in their calculations emission profiles obtained from nitrogen discharges. As already explained earlier, these profiles present two maxima located near the electrodes and are probably close to the silane emission profiles in the γ regime. However, since the sheath sizes, and consequently the exact location of the maxima, depend on the nature of the gas, this assumption can induce some error in these calculations. Besides it is clear from the previous discussion that at least in the α regime one should use LIF profiles instead of emission.³⁶ However, it is suggested that in the γ regime LIF profiles would probably be closer to emission profiles than in the α regime, but this remains to be seen in future experiments.

The phenomena observed will certainly affect the gas phase composition and the *a*-Si:H deposition mechanism. The latter will change to the extent that the availability of various radicals to surface processes will be different. This group has already reported results showing a direct relation of interelectrode distance with the deposition rate the defect density of *a*-Si:H films deposited under the same conditions.³⁷ In this case, deposition rate does not increase continuously with the decrease of *d*, but presents a maximum at *d* = 27 mm at 50 mTorr, or a tendency for saturation from the same *d* at 100 mTorr. This distance coincides with the inflection point of the LIF curves (Fig. 7) indicating a possible correlation between a change in the deposition mechanism and the phenomena observed here.

V. CONCLUSIONS

Generally, the variation of the basic geometric characteristics of a silane discharge influences all the primary processes, which occur by electron molecule collisions. This is the case because the electron energy distribution, as a function of space and time, is affected.

In the present study this influence, on dissociation and dissociative excitation processes, has been identified by monitoring the spatial distribution and behavior of SiH and SiH*. There are several differences in the response of these species to geometry variations, in conjunction with pressure and power density, which lead to the conclusion that the production of SiH* depends mainly on the sheath characteristics whereas the production of SiH depends on the power density in the bulk. It is supported by the present results that the behavior of SiH is representative

for all the other ground state radicals. Thus, normalized LIF spatial profiles can be effectively used as the spatially distributed source of radicals, in the range of our working conditions, in order to calculate the spatial concentration profiles of each radical as well as the composition of the flux incident to the deposition surface.

Secondary gas phase processes, as radical-neutral and radical-radical reactions, are also influenced by the discharge geometry as silane depletion and/or residence time are affected.

The resulting modification of the gas phase composition by primary and secondary processes is affecting the deposition rate and the quality of the film. Thus, the chamber geometry has also significant effects on the deposition mechanism.

ACKNOWLEDGMENTS

The authors wish to thank Dr. J. Perrin for the stimulating conversations. This work was supported by the "JOULE I" R&D program of the Commission of European Communities, DG XII.

- ¹J. P. M. Schmitt, P. Gressier, M. Krishnan, G. De Rosny, and J. Perrin, *Chem. Phys.* **84**, 281 (1984).
- ²G. Inoue and M. Suzuki, *Chem. Phys. Lett.* **105**, 641 (1984).
- ³R. M. Roth, K. G. Spears, and G. Wong, *Appl. Phys. Lett.* **45**, 28 (1984).
- ⁴N. Itabashi, K. Kato, N. Nishiwaki, T. Goto, C. Yamada, and E. Hirota, *Jpn. J. Appl. Phys.* **27**, L1565 (1988).
- ⁵N. Itabashi, K. Kato, N. Nishiwaki, T. Goto, C. Yamada, and E. Hirota, *Jpn. J. Appl. Phys.* **28**, L325 (1989).
- ⁶D. Mataras, S. Cavadias, and D. Rapakoulias, *J. Appl. Phys.* **66**, 119 (1989).
- ⁷D. Mataras, S. Cavadias, and D. E. Rapakoulias, in *Proceedings of the 9th International Symposium on Plasma Chemistry*, Pugnochiuso, 1989, edited by R. D'Agostino (IUPAC, Pugnochiuso, 1989), p. 423.
- ⁸S. Ishihara, M. Kitagawa, T. Hirao, and K. Wasa, *J. Appl. Phys.* **62**, 485 (1987).
- ⁹R. C. Ross, and J. Jaklik, Jr., *J. Appl. Phys.* **55**, 3785 (1984).
- ¹⁰T. Hamasaki, M. Ueda, A. Chayahara, M. Hirose, and Y. Osaka, *Appl. Phys. Lett.* **44**, 600 (1984).
- ¹¹F. H. Karg, H. Bohm, and K. Pierz, *J. Non-Cryst. Solids* **114**, 477 (1989).
- ¹²K. Kohler, J. W. Koburn, D. E. Horne, and E. Kay, *J. Appl. Phys.* **57**, 59 (1984).
- ¹³D. E. Gerassimou, S. Cavadias, D. Mataras, and D. E. Rapakoulias, *J. Appl. Phys.* **67**, 146 (1990).
- ¹⁴R. A. Gottscho, G. R. Scheller, D. Stoneback, and T. Intrator, *J. Appl. Phys.* **66**, 492 (1989).
- ¹⁵K. Tachibana, T. Mukai, A. Yuuki, Y. Matsui, and H. Harima, *Jpn. J. Appl. Phys.* **29**, 2156 (1990).
- ¹⁶F. Tochikubo, A. Suzuki, S. Kakuta, Y. Terazono, and T. Makabe, *J. Appl. Phys.* **68**, 5532 (1990).
- ¹⁷B. Chapman, *Glow Discharge Processes* (Wiley, New York, 1980).
- ¹⁸G. Turban, in *Interactions Plasma Froids Materiaux*, edited by C. Leu-jeune (Les Editions de Physique, Les Ulis, France, 1988), p. 79.
- ¹⁹J. P. M. Schmitt, *J. Non-Cryst. Solids* **59&60**, 649 (1983).
- ²⁰A. Gallagher, *J. Appl. Phys.* **63**, 2406 (1988).
- ²¹N. Itabashi, N. Nishiwaki, M. Magane, S. Naito, T. Goto, A. Matsuda, C. Yamada, and E. Hirota, *Jpn. J. Appl. Phys.* **29**, L505 (1990).
- ²²J. Perrin and J. F. M. Aarts, *Chem. Phys.* **80**, 351 (1983).
- ²³C. Chan, Z. Jin, and C. Whitaker, *J. Appl. Phys.* **62**, 1633 (1987).
- ²⁴D. B. Graves, *J. Appl. Phys.* **62**, 88 (1987).
- ²⁵O. A. Popov and V. A. Godyak, *J. Appl. Phys.* **57**, 53 (1985).
- ²⁶M. J. Kushner, *J. Appl. Phys.* **54**, 4958 (1983).

- ²⁷A. Garscadden, G. L. Duke, and W. F. Bailey, *Appl. Phys. Lett.* **43**, 1012 (1983).
- ²⁸A. J. van Roosmalen, W. G. M. van den Hoek, and H. Kalter, *J. Appl. Phys.* **58**, 653 (1985).
- ²⁹R. M. Roth, *Mater. Res. Soc. Symp. Proc.* **98**, 209 (1987).
- ³⁰T. Bisschops, P. M. Vallinga, C. V. Van den Berghe, and P. M. Meijer, in *Proceedings of the 8th International Symposium on Plasma Chemistry*, Tokyo, 1987, edited by K. Akashi and A. Kinbara (IUPAC, Tokyo, 1987), p. 614.
- ³¹P. Bletzinger and S. De Joseph, *IEEE Trans. Plasma Sci.* **PS-14**, 124 (1986).
- ³²Z. J. Jin, C. Chan, and C. Whitaker, *Rev. Sci. Instrum.* **59**, 427 (1988).
- ³³J. Perrin, P. Roca i Cabarrocas, B. Allain, and J. M. Friedt, *Jpn. J. Appl. Phys.* **27**, 2041 (1988).
- ³⁴V. A. Godyak and A. S. Khanneh, *IEEE Trans. Plasma Sci.* **PS-14**, 112 (1986).
- ³⁵V. I. Kuznetsov, R. C. van Oort, and J. W. Metselaar, *J. Appl. Phys.* **65**, 575 (1989).
- ³⁶D. Mataras, S. Cavadias, and D. Rapakoulias, *Mater. Res. Soc. Symp. Proc.* **165**, 55 (1990).
- ³⁷P. Kounavis, E. Mytilineou, D. Mataras, S. Cavadias, and D. Rapakoulias, in *Proceedings of the 20th International Conference on the Physics of Semiconductors*, Thessaloniki, 1990, edited by E. M. Anastasakis and G. D. Joannopoulos (World Scientific, Singapore, 1990), p. 2115.